ADVANCES IN ATMOSPHERIC SCIENCES, VOL. 27, NO. 2, 2010, 265–273

The Cold Tongue in the South China Sea during Boreal Winter and Its Interaction with the Atmosphere

Hamza VARIKODEN*, A. A. SAMAH, and C. A. BABU

National Antarctic Research Centre, University of Malaya, IPS Building, Kuala Lumpur-50603, Malaysia

(Received 9 September 2008; revised 14 May 2009)

ABSTRACT

A distinct cold tongue has recently been noticed in the South China Sea during the winter monsoon, with the cold tongue temperature minimum occurring in the January or February. This cold tongue shows significant links with the Maritime Continent's rainfall during the winter period. The cold tongue and its interaction with the Maritime Continent's weather were studied using Reynolds SST data, wind fields from the NCEP–NCAR reanalysis dataset and the quikSCAT dataset. In addition, rainfall from the GOES Precipitation Index (GPI) for the periods 2000 to 2008 was also used. The propagation of the cold tongue towards the south is explained using wind dynamics and the western boundary current. During the period of strong cold tongue, the surface wind is strong and the western boundary current advects the cold tongue to the south. During the period of strong winds the zonal gradient of SST is high [0.5°C (25 km)$^{-1}$]. The cold tongue plays an important role in regulating the climate over the Maritime Continent. It creates a zonal/meridional SST gradient and this gradient ultimately leads in the formation of convection. Hence, two maximum precipitation zones are found in the Maritime Continent, with a zone of relatively lower precipitation between, which coincides with the cold tongue's regions. It was found that the precipitation zones have strong links with the intensity of the cold tongue. During stronger cold tongue periods the precipitation on either side of the cold tongue is considerably greater than during weaker cold tongue periods. The features of convection on the eastern and western sides of the cold tongue behave differently. On the eastern side convection is preceded by one day with SST gradient, while on the western side it is four days.

Key words: cold tongue, SST gradient, wind, precipitation

Citation: Varikoden, H., A. A. Samah, and C. A. Babu, 2010: The cold tongue in the South China Sea during boreal winter and its interaction with the atmosphere. *Adv. Atmos. Sci.*, **27**(2), 265–273, doi: 10.1007/s00376-009-8141-4.

1. Introduction

The South China Sea (SCS) is the largest marginal sea in Southeast Asia, with a basin deeper than 4000 m in the central region and surrounded by a large continental shelf of less than 200 m in depth (Shaw and Chao, 1994). It is connected with the East China Sea to the northeast, the Pacific and the Sulu Sea to the east, and the Java Sea and Indian Ocean to the southwest. The SCS is an integral part of the East Asian monsoon system (Wyrtki, 1961; Lau et al., 1998). The SST of the SCS is an important factor in the development and evolution of the East Asian monsoon. Many studies have revealed that the SCS SST shows an interannual variation that is closely associated with the interannual variation of the East Asian monsoon (Shen and Lau, 1995; Tomitha and Yasunari, 1996; Chu and Chang, 1997; Wen et al., 2000) and also with ENSO episodes (Lim and Tuen, 1991; Liu et al., 2004). Lim and Tuen (1991) reported that the SCS SST shows marked intraseasonal and interannual variabilities and suggested more detailed studies for linking these variabilities with weather events in the SCS and neighboring continents. In the SCS the seasons play a vital role for regulating SST. In winter the SCS is dominated by strong northeasterly winds, whereas in summer the di-

*Corresponding author: Hamza VARIKODEN, hamzavarikoden@gmail.com
Current affiliation: Climatology and Hydrometeorology Division, Indian Institute of Tropical Meteorology, Pashan, Pune 411 008, India

rection turns to southwesterly (Liu and Xie, 1999). A summer upwelling was reported by Xie et al. (2003) along the Vietnam coast in association with Ekman pumping as a result of southwesterly alongshore surface winds (Kuo et al., 2000). The cooling of SST over the SCS during the winter monsoon is yet to be properly documented, even though some studies have been carried out by Lim and Tuen (1991).

Recently, a new high resolution SST data from satellite has been used in ocean research and found a winter cold tongue (Liu et al., 2004) and a summer cold filament (Xie et al., 2003) in the SCS. Liu et al. (2004) investigated the seasonal development of this cold tongue and attributed the mechanism for its southward movement to the western boundary current along the Vietnam coast. The authors further reported that the cold tongue is fully developed by November, along with the western boundary currents. The interannual variability of the SCS SST shows a phase-to-phase relationship with SST anomalies in the Niño-3 area, while the reverse is true in the tropical west Pacific (Liu et al., 2004). The authors' analysis revealed that a cold tongue band developed further up until the end of February, even though an overall cooling was noticed in the SCS. This cold tongue acts as a conspicuous discontinuity of the warm ocean over the Indo-Pacific region (Liu et al., 2004).

In this paper the monthly evolution of the cold tongue formed over the SCS during the boreal winter season is described, and the role of the cold tongue in the regulation of atmospheric phenomena is addressed. The cold band of SST divides the SCS into two warm oceans: one on the eastern side—the Gulf of Thailand; and the other on the western side—the central SCS. It is found that zonal SST gradients play a major role in the development of the winter climate over the Maritime Continent. An attempt is also made to differentiate between the changes in rainfall pattern during strong and weak cold tongue periods. The findings of this work will be beneficial in understanding the SCS SST climatology and its interaction with the maritime continent and nearby seas.

2. Data and methodology

The present study utilizes the daily Reynolds SST dataset over the SCS for the period 2000–2008. This dataset has a latitude–longitude spatial resolution of $0.25^\circ \times 0.25^\circ$ (Reynolds et al., 2007) and has been developed using the optimum interpolation (OI) technique. The analyses have a spatial grid resolution of 0.25° and a temporal resolution of one day. The product uses Advanced Very High Resolution Radiometer (AVHRR) infrared satellite SST data and the NASA Earth Observing System satellite—Advanced Microwave Scanning Radiometer (AMSR) SST data. Both of these also use *in situ* data from ships and buoys and include a large-scale adjustment of satellite biases with respect to the *in situ* data. Because of the AMSR's near all-weather coverage, there is an increase in OI signal variance when it is combined with AVHRR data. The AVHRR-only product uses Pathfinder AVHRR data (currently available from January 1985 through December 2005) and operational AVHRR data from 2006 onwards.

In addition to the Reynolds SST dataset, the NCEP–NCAR wind dataset was used in order to understand the dynamic behavior of the atmosphere over the cold tongue region in the SCS. This dataset has a spatial resolution of $2.5^\circ \times 2.5^\circ$ grid with and a temporal resolution of one day. Even though the wind data is model-derived, it is well related to observed data and hence it is in the most reliable class of measured wind observations (Kalnay et al., 1996). Similarly, although the spatial resolution is comparatively low, this dataset well represents the real picture of the atmosphere on the synoptic scale.

GOES precipitation index (GPI) data were also used to understand the spatial and temporal distribution of rainfall during the cold tongue period and also to relate the SST gradient with precipitation in the Maritime Continent. The satellite-derived GPI is a good measure of the daily rainfall on a $1^\circ \times 1^\circ$ regular grid for the period 1997 to present. This daily precipitation estimation technique is a complete first generation procedure for estimating global daily precipitation (Huffman et al., 2001). The primary source of information over the tropical oceans is infrared data from polar-orbiting and geostationary satellites. The estimates are generated using a cloud top temperature-thresholding algorithm. This method of using satellite-observed cloud top brightness temperatures to infer areas of deep convection was demonstrated by Arkin (1979) using data from the Global Atmosphere Research Program (GARP) Atlantic Tropical Experiment (GATE). As an indirect measure of rainfall, the GPI infers tropical rainfall rates from the long wave radiation flux at the top of the atmosphere based on the inverse relationship that exists between radiance and rainfall. In this study, as a measure of tropical precipitation, GPI data for a period 2000–2008 have been used.

QuikSCAT surface wind data (spatial resolution of $0.25^\circ \times 0.25^\circ$ and available daily) were utilized to identify wind stress features and wind stress curl. The wind stress curl is an indirect method to understand the features of Ekman pumping (Munchow, 2000). To estimate surface wind stress (τ) the bulk formulation

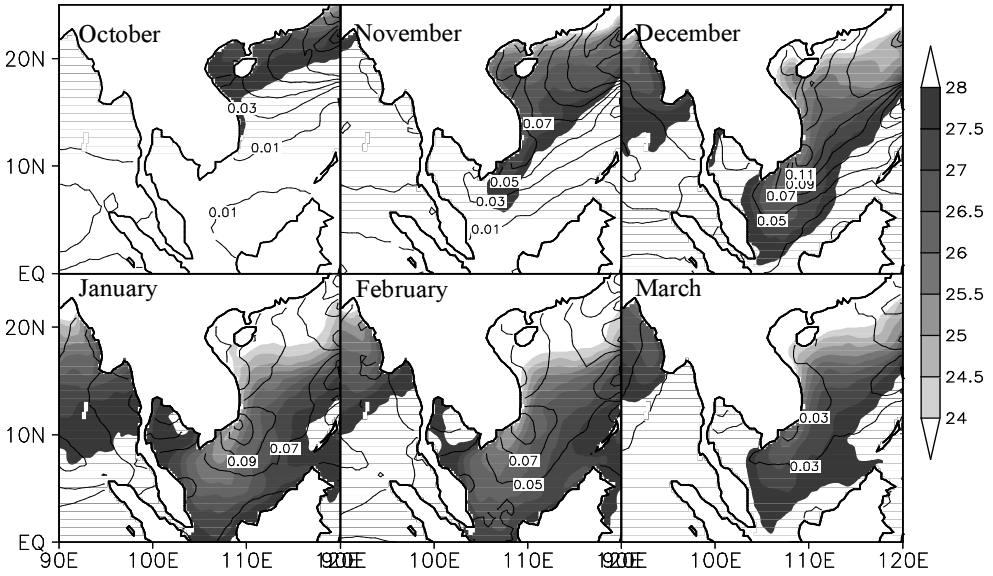

Fig. 1. Multiyear average (2000–2008) of Reynolds SST in the SCS from October to March. Overlaid contours represent surface wind stress (N m^{-2}) and shaded areas indicate SST between 24° and 28°.

is used:

$$|\tau| = \rho C_{\mathrm{d}} |V| \boldsymbol{V}$$

where ρ is the density of air (1.225 kg m^{-3}), C_{d} is the drag coefficient (0.0013), and $\boldsymbol{V}$ is the wind velocity. The equation for wind stress curl is:

$$\mathrm{Curl} = \frac{\Delta \tau_y}{\Delta x} - \frac{\Delta \tau_x}{\Delta y}$$

where τ_y and τ_x are the meridional and zonal components of wind stress, respectively.

3. Results and discussion

3.1 *Climatology of the SCS cold tongue and its evolution*

The multiyear averaged spatial distribution of SST during the boreal winter months over the SCS shows a distinct cold tongue (CT) from the Vietnam coast to the equatorial region through to the Sunda Shelf (Fig. 1). A threshold isotherm value of 28°C is used to distinguish the CT from the surrounding warm water. The CT propagates further towards the south in consecutive months and reaches a latitude of 2°N through the Sunda Shelf by the end of January/early February. The maximum intensity of the CT is noticed over the Sunda Shelf, even though a wide range of cooling of the SCS is noticed in association with radiational cooling of the winter monsoon. The propagation of the CT towards the south beyond the Sunda Shelf is governed by atmospheric dynamics, mainly surface wind. The surface wind stress from the quikSCAT wind products is overlaid in Fig. 1 as contours with an interval of 0.02 N m^{-2}. This shows that the wind stress is high over the area of low SST, especially along the Vietnam coast where the SST is lower than elsewhere. This indicates that an external force is acting on the water surface which causes the downwelling of ocean water. The maximum wind stress is seen during the months of December and January over the Vietnam coast (values exceed 0.1 N m^{-2}) and this is due to the strong wind during these periods. The zonal gradient of SST is also high during these months and exactly over the same area.

Another feature noticed in the SST distribution is cold water tightening in the coastal region and propagation of warm water towards the coast during the peak boreal winter months. The SST gradient is high during the month of January because the wind over the region is almost parallel to the coast and this alongshore wind amplifies the sinking motion due to downwelling (Pickard and Emery, 1992). This downwelling also supports the negative value for surface wind stress curl and similar results were reported by Shaw et al. (1999). The zonal gradient of SST shows a maximum near the coastal region where the wind stress is also at a maximum and the wind stress curl is negative. A composite SST zonal gradient and wind stress curl for eight years is given in Fig. 2. The zonal gradient of SST ($d(\mathrm{SST})/dx$) is presented in shaded colors and the wind stress curl (10^{-7} N m^{-3}) is presented as contours. Hamza et al. (2007) studied the seasonal variation of wind stress curl over the Indian Ocean and

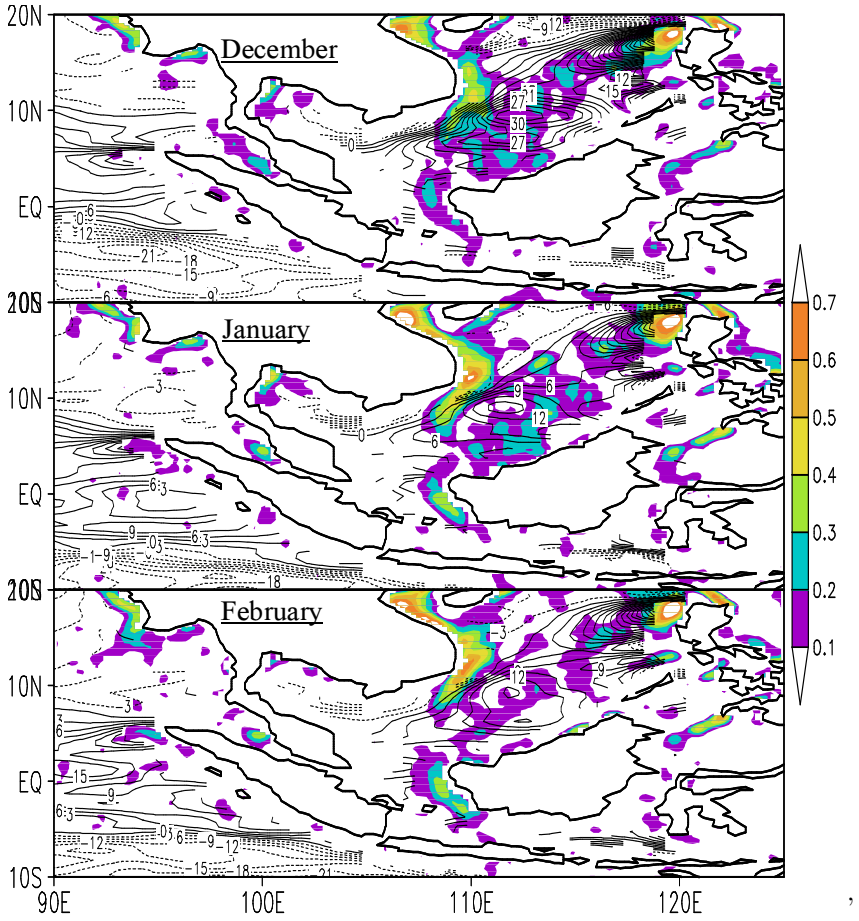

Fig. 2. Multiyear average of zonal gradient of SST [°C (25 km)$^{-1}$] during December, January and February. Contours represent the surface wind stress curl (10^{-7} N m^{-3}) during the period, indicating downwelling (negative values are represented by dashed lines) of surface water near the Vietnam coast where the high zonal gradient of SST exists.

found that a positive curl exists over the equatorial Bay of Bengal during the winter season, indicating upwelling. In the case of the SCS, positive values are prominent as a measure of upwelling during the winter season except over the Vietnam coast. In the coastal zone of Vietnam, the rate of decrease of zonal SST during January is greater than 0.5°C (25 km)$^{-1}$ near to the coast (12.5°N and 110°E) but decreases away from the coast. This large gradient of SST in the coastal areas indicates the rate of sinking. The mechanism for equatorial transport of this cold water from the Vietnam coast and Sunda Shelf can be explained based on the surface wind pattern.

Figure 3 shows the area average time series of SST over CT regions and non-CT regions. The CT region is taken as the area over the box 7°–10°N and 105°–110°E, in which the cold water is advected from the Vietnam coast as a result of the western boundary current and Ekman pumping (Liu et al., 2004). The non-CT region is taken as the area over the box 7°–10°N and 110°–114°E in the Central SCS (CSCS), where

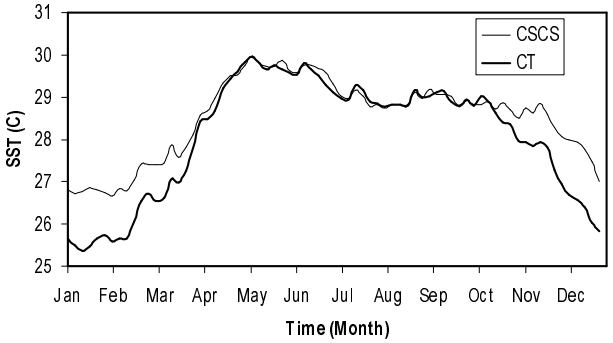

Fig. 3. Multiyear average time series of SST in the CT regions (area average over 7°–10°N and 105°–110°E) and in the CSCS (area average over 6°–10°N and 110°–114°E). Pentads are plotted in the time series to remove high frequency fluctuations.

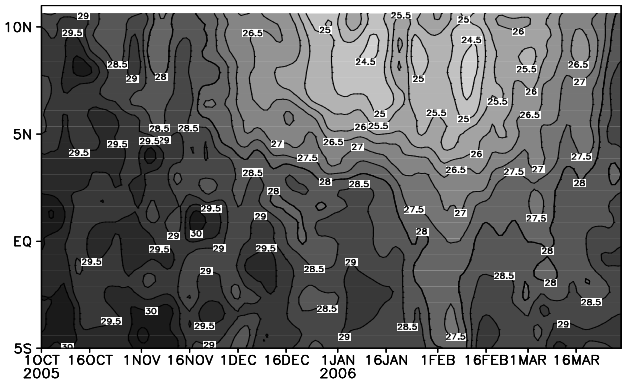

Fig. 4. Latitudinal cross section of SST averaged over the longitudinal belt 106°–108°E for the year 2005/2006. Development and further intensification of the CT can be observed.

the SST gradient is smallest. This is due to the CT, as explained in Fig. 2. The strength of the CT can be measured using the SST gradient between the CT area and non-CT area. The SST gradient between the CT region and CSCS region starts to develop from early October. The SST gradient during summer months is negligible because SST distribution during the summer season is almost uniform across the entire SCS (the maximum difference is 0.3°C). But during the summer season, a warm pool was reported in the area between 7°–12°N and 111°–116°E (SST > 30.5°C) by Chu and Chang (1997). However, during the summer season, there is not much difference between the SST in the CSCS and the CT region in the warm pool period because the SST in both regions is above 30°C. Therefore, the SST gradient is the smallest during the summer monsoon months. A difference in SST between these two regions starts to evolve from early October. After the formation of the CT, SST over the CT region decreases further and reaches a minimum of 25.3°C in the second week of January. The average SST during the period of November through March over the CT region is 26.9°C, with a standard deviation of 1.1°C. The average slope of SST in the CT region is 0.25°C month^{-1}, while that in the CSCS is only 0.0006°C month^{-1}. This indicates that the rate of decrease of SST is much greater over the CT region due to the formation of the cold tongue. From the graph, it is clear that the decrease in temperature continues up to the end of January and then starts to increase the SST due to the net surface heating caused by solar radiation (Chen et al., 2003).

In order to verify the CT features, we created a latitudinal cross section of SST over the longitude belt 106°–108°E during the boreal winter months of 2005/2006. In Fig. 3 the 28°C isotherm was plotted as a thick line to easily identify the propagation of the CT. In this representative year a band of cold water of 28°C started to build up in the early days of November. It propagated toward the south up to 7.7°N and dissipated thereafter. Around the middle of November the CT started to build up again and propagated continuously towards the south. The propagation of this CT up to the Sunda Shelf (3°N) was a rapid process. The advection of cold water from the southern Vietnam coast to the southern edge of the Sunda Shelf took place within a short span of two weeks. The CT continued to propagate further to the south, with the 28°C isotherm (or < 28°C) reaching around 5°S during late January/early February. It remained there for two weeks with a small temporal variability. This southward movement of the CT beyond the equator can be seen in all years during late January or early February. After the second week of February the cold water begins to retreat to its ambient value. The rate of increase of SST with respect to time is higher than that of the rate of decrease. From the second week of February, the cold water in the region is replaced with warm water within a month. Hence, by the third week of March the entire SCS SST becomes more than 28°C.

3.2 *Wind characteristics during the cold tongue period*

It is well known that SST cooling is governed by different mechanisms in the above few meters of the ocean surface. Cooling of the ocean surface is either due to oceanic processes, atmospheric dynamics, or both (Chen et al., 2003). The relative importance of the cooling mechanism is different for different geographical locations and for different seasons (Duing and Leetma, 1980; Rao et al., 1989; Rao and Sivakumar, 2000; Shenoi et al., 2002). The multiyear (2000–2008) averaged wind fields at 925 hPa during boreal winter (Fig. 5) show the occurrence of strong northeasterlies from November to February. In the month of October, the remnants of the southwest monsoon still prevail in the southern SCS as southwesterly winds. However, the wind turns northeasterly in the northern part of the SCS beyond 12°N by October. This northeasterly wind develops well and moves towards the south to establish the boreal winter monsoon. Strong winds of >12 m s^{-1} are seen along the Vietnam coast, with the wind being almost parallel to the coast. This parallel wind contributes further to the propagation of the CT towards the south. Even after the full establishment of the western boundary current along the Vietnam coast by November, it was noticed that the propagation of the CT towards the south continues and this southward propagation might be attributed

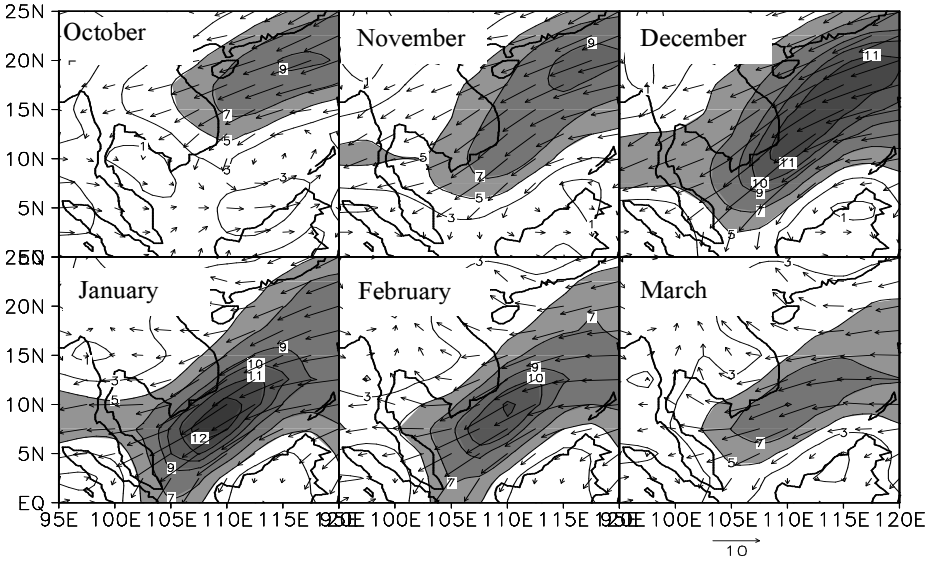

Fig. 5. Multiyear average of wind at 925 hPa during the CT period. Wind magnitude >5 m s^{-1} is shaded. The direction of the wind can be read from the vector of the wind.

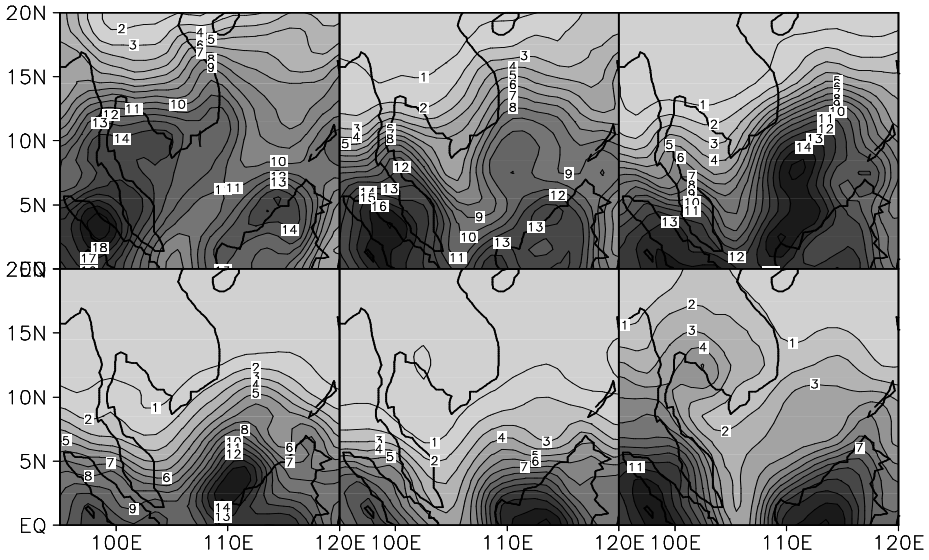

Fig. 6. Multiyear average (2000–2008) precipitation climatology from October to March derived from the GPI. The interval is 1 mm and the units are mm d^{-1}.

to northerly winds. By January/February the southward extension of strong winds (speeds of >7 m s^{-1}) reaches the equator, often crosses it. Surface waters with low SST also move along with this wind during the months of December to February. A strong alongshore component of the wind in the coastal belt favours downwelling, as discussed above, in relation with the surface wind stress curl in the coastal belt of Vietnam. The zonal gradient of SST is large in this strong wind belt, indicating a sharp reduction in SST towards the coast. By the month of March, the wind strength starts to decrease and the average wind speed in the SCS reaches 5 m s^{-1}. Due to this reduced wind strength and increased net heat flux, the CT starts to dissipate.

3.3 *Distribution of precipitation*

The multiyear average (2000–2008) of monthly GPI precipitation as a measure of rainfall in mm d^{-1} is given in Fig. 6. The spatial distribution of the rainfall pattern shows similarities with the CT region of the SCS. During October, the precipitation band is more or less distributed uniformly in the SCS, even though two prominent rain bands are seen: one over the Suma-

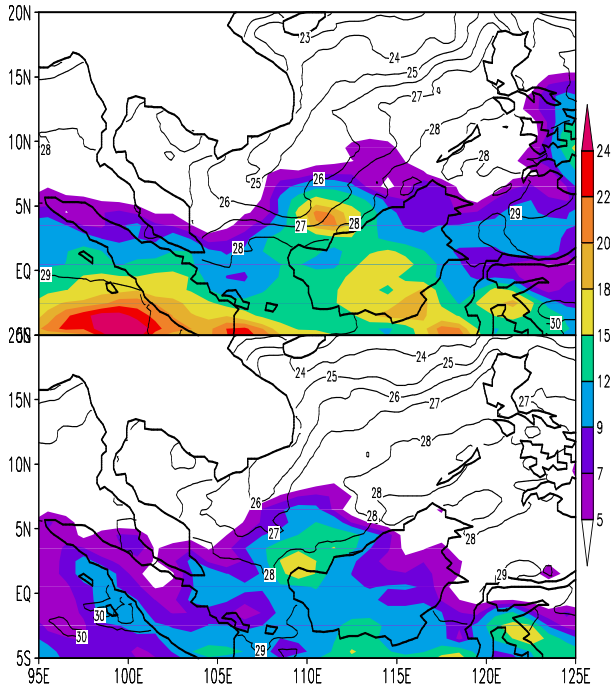

Fig. 7. SST and GPI rainfall (mm d-1) during strong and weak CT periods. During strong periods the rain bands on both sides of the CT are strong, while during weak periods the rain zones on both sides are weak.

tra region and another over the Borneo region. The mean monthly distribution of precipitation is associated with the remnants of the summer monsoon season over the region, which can also be seen in the wind fields. From November onwards the distribution of rainfall is different to that of October. In the SCS, the isohyets show a trough near the CT region. This low precipitation zone indicates a lack of convection in the low SST region. Either side of the CT, however, two prominent precipitation zones can be seen. These precipitation zones are associated with the temperature gradient between the CT region with adjoining warm seas in the east and in the west. Joseph et al. (2005) and Joseph and Sabin (2008) reported similar SST gradient–convection relationships over the Bay of Bengal during the southwest monsoon season. These precipitation zones provide an overall picture of the interrelation between the CT and rainfall.

To understand the features of precipitation between the strong and weak CT periods, the authors examined SST and GPI rainfall for the periods 1 January to 30 January 2006 (representing a strong CT) and from 1 January to 30 January 2003 (representing a weak CT). The strong and weak CT periods were identified based on SST differences between the CT area and the CSCS area, as described in the Section 3.1. During the strong CT period, the rainfall amount was considerably high on both the Borneo and Sumatra sides, as compared to weak CT periods (Fig. 7). In strong periods, rainfall over the Sumatra region exceeds 24 mm d^{-1}, and over Borneo region it exceeds 20 mm d^{-1}. The SST in the CT area is less than 25°C. However, during weak CT periods, rainfall is less on both the Borneo and Sumatra sides. On the Borneo side, rainfall is about 15 mm d^{-1}, while on the Sumatra side it is less than 12 mm d^{-1}. In both cases, a rain shadow area indicating less convection is noticed over the CT region. This indicates a strong dependence of the CT on rainfall. This strong dependence suggests that the zonal gradient of SST over the SCS plays a vital role in regulating rainfall over the Sumatra and Borneo regions.

The linear correlation coefficient (LCC) of GPI rain over the box area 96°–102°E and 0°–7°N (representing the western side, Sumatra region) with the SST gradient between the CT region (7°–10°N and 105°–110°E) and its western side (3°–6°N and 103°–106°E), and similarly the LCC of GPI rain over the Borneo side (0°–5°N and 109°–115°E) with the SST gradient between the CT region (7°–10°N and 105°–110°E) and its eastern side (3°–7°N and 110°–115°E) are examined and presented in Fig. 8. In Fig. 8 negative values on the x-axis represent the lag of precipitation with the SST gradient and positive values represents its lead. The convection in the western side of the CT is led by one day (LCC=0.4), and the convection is triggered after one day following the formation of the SST gradient between the regions. However, the LCC between the eastern side GPI and the SST gradient shows a different picture. In this case, the 12-day periodicity of precipitation can be seen. The maximum LCC is found on either side of the lead and lag. The lag correlation maximum is found at eight days and

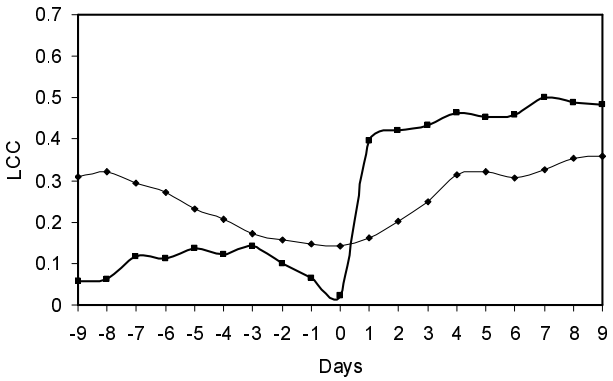

Fig. 8. LCC between SST gradient between the CT and the western side of the CT with GPI over the western side (sold line with diagonal dots) and the SST gradient between the CT region and the eastern side with the GPI over the western side (thick sold line with square dots).

the lead correlation maximum at four days. This indirectly shows that the precipitation's convection forms four days after the build up of the SST gradient. The precipitation due to this SST gradient cools the ocean further. The SST gradient builds up again after eight days following the maximum level of convection. To establish a strong theory between the SST gradient and precipitation more studies on ocean atmosphere interaction involving radiation and surface fluxes are needed.

4. Conclusions

During the boreal winter monsoon season, a well developed CT is observed in the SCS near the Vietnam coast and along the Sunda Shelf and further beyond to the south. This CT extends towards the Sunda Shelf (the bathymetry of the Sunda Shelf is <200 m) by the end of November. The southward movement of the CT is attributed to the western boundary current along the Vietnam coast. It further extends towards the south, sometimes even crossing the equator and reaches up to 5°S by January or February. The cooling of the CT region is slower during the formation of the CT in comparison with the rate of warming of the region during dissipation of the CT. The average SST of the CT regions is 26.9°C, with a standard deviation 1.1°C. A similar extension of the wind field is also seen in the same region as that of the CT in the SCS. The coherence of near surface wind fields and SST can be explained as the mechanism for the propagation. In the boreal winter monsoon season temperature over the CT region reaches a minimum value of 24.5°C in the months of January and February, with small variability.

The southward propagation of the CT is controlled by the surface wind. The wind strength reaches >12 m s^{-1} during January in the coastal belt of Vietnam; the southward extension of strong winds were also noticed during this month, advecting cold water towards the south. During the period of strong winds, in January and February, the zonal gradient of SST is large along the coastal belt, indicating a tightening of the SST in the coastal region, which causes the downwelling of cold water to the subsurface. This downwelling of surface water is supported by a negative wind stress curl and a high wind stress over the sinking area.

The CT plays a vital role in regulating the climate over the Maritime Continent. The relation of the CT with convection was also studied in order to understand the role of the CT in the formation of rainfall in the Maritime Continent. Two prominent precipitation zones were identified, one over the Sumatra region on the western side and another over the Borneo region on the eastern side. These precipitation zones show strong links with the zonal gradient of SST across the SCS. During strong periods rainfall is higher, as compared to weak periods of CT SST. On the Borneo side, rainfall exceeds 20 mm d^{-1} during strong periods; however, it is less than 12 mm d^{-1} in most places during weak periods. Convection on the eastern side is led by one day by the SST gradient. However, on the western side, it is led by four days; plus, a strong correlation value is found on the lag side (eight days) as well. This lead–lag correlation represents a 12-day periodicity of convection and SST gradient.

Acknowledgements. The second author is thankful to the eScience Fund Project (No. 04-01-03-SF0410) for the financial support and all authors are grateful to the University of Malaya for providing facilities. Comments from two reviewers have helped to improve the manuscript. The first author is grateful to the Director, Indian Institute of Tropical Meteorology for providing facilities and other required support to do the revision of this manuscript.

REFERENCES

Arkin, P. A., 1979: The relationship between fractional coverage of high cloud and rainfall accumulations during GATE over the B-scale array. *Mon. Wea. Rev.*, **106**, 1153–1171.

Chen, J.-M., C.-P. Chang, and T. Li, 2003: Annual cycle of the South China Sea surface temperature using the NCEP/NCAR reanalysis. *J. Meteor. Soc. Japan*, **81**, 879–884.

Chu, C. P, and C.-P. Chang, 1997: South China Sea warm pool in boreal spring. *Adv. Atmos. Sci.*, **14**, 195–206.

Chu, P. C., S. Lu, and Y. Chen, 1997: Temporal and spatial variabilities of the South China Sea surface temperature anomaly. *J. Geophys. Res.*, **102-C9**, 20937–20955.

Duing, W., and A. Leetma, 1980: Arabian Sea cooling: A preliminary heat budget. *J. Phys. Oceanogr.,* **10**, 307–312.

Hamza, V., C. A. Babu, and T. P. Sabin, 2007: Characteristic study of the boundary layer parameters over the Arabian Sea and the Bay of Bengal using quikSCAT dataset**.** *Adv. Atmos. Sci.*, **24,** 631–643.

Huffman, G. J., R. F. Adler, M. M. Morrissey, D. T. Bolvin, S. Curtis, R. Joyce, B. Mcgavock, and J. Susskind, 2001: Global precipitation at one degree daily resolution from multisatellite observations. *Journal of Hydrometeorology.*, **2**, 36–50.

Joseph, P. V., and T. P. Sabin, 2008: An ocean atmosphere interaction mechanism for the active break cycle of the Indian summer monsoon. *Climate Dyn.*, **30**(6), 553–566, doi: 10.1007/s00382-007-0305-2.

Joseph, P. V., K. P. Sooraj, C. A. Babu, and T. P. Sabin, 2005: A cold pool in the Bay of Bengal and its inter-

action with active break cycle of the monsoon. *Clivar Exchanges*, **10**(3), 10–12.

Kalnay, E., and Coauthors, 1996: The NCEP/NCAR 40 year reanalysis project. *Bull. Amer. Meteor. Soc.*, **77**, 437– 471.

Kuo, N.–J., Q. Zheng, and C.–R Ho, 2000: Satellite observation of upwelling along the western coast of South China Sea. *Remote Sens. Environ.*, **74**, 463–40.

Lau, K.-M., H.–T Wu, and S. Yang, 1998: Hydrologic processes associated with the first transition of the Asian summer monsoon: A pilot satellite study. *Bull. Amer. Meteor. Soc.*, **79**, 1871–1882.

Lim, J. T, and K. L. Tuen, 1991: Sea surface temperature variations in the South China Sea during the northern hemisphere winter monsoon. *Proceedings of the Second Pacific Symposium,* Penag, Malaysia, 113–144.

Liu, Q., X. Jiang, S.–P. Xie, and W. T. Liu, 2004: A gap in the Indo-Pacific warm pool over the South China Sea in boreal winter: Seasonal development and interannual variability. *J. Geophys. Res.*, **109**, C07012, doi: 10.1029/2003JC002179.

Liu, W. T., and X. Xie, 1999: Space based observations of the seasonal changes of the south Asian monsoon and oceanic responses. *Geophys. Res. Lett.*, **26**, 1473–1476.

Münchow, A., 2000: Wind-stress curl forcing of the coastal ocean near Point Conception, California. *J. Phys. Oceanogr.*, **30**, 1265–1280.

Pickard, G. L., and J. W. Emery, 1992: *Descriptive Physical Oceanography, An Introduction* (*5th Edition*). Butterworth-Heinemann, Oxford, 320pp.

Rao, R. R., and R. Sivakumar, 2000: Seasonal variability of near-surface thermal structure and heat budget of the mixed layer of the tropical Indian Ocean. *J. Geophys. Res.*, **108**(C1), 995–1015.

Rao, R. R., R. L. Molinari, and J. F. Festa, 1989: Evolution of the climatological near-surface thermal structure of the tropical Indian Ocean, I, description of mean monthly mixed layer depth, and sea surface temperature, surface currents, and surface meteorological fields. *J. Geophys. Res.*, **94**(C10), 10801–10815.

Reynolds, R. W., C. Liu, T. M. Smith, D. B. Chelton, M. G. Schlax, and K. S. Casey, 2007: Daily high-resolution-blended analyses for sea surface temperature. *J. Climate*, **20**(22), 5473–5496, doi: 10.1175/2007JCLI1824.1.

Shaw, P. T., and S. Y. Chao, 1994: Surface circulation in the South China Sea. *Deep-Sea Res.*, **40**(11/12), 1663–1683.

Shaw, P. T., S. Y. Chao, and L. Fu, 1999: Sea surface height variations in the South China Sea from satellite altimetry. *Oceanologica Acta*, **22**, 1–17.

Shen, S., and K.–M. Lau, 1995: Biennial oscillation associated with the East Asian summer monsoon and tropical sea surface temperature. *J. Meteor. Soc. Japan*, **73**, 105–124.

Shenoi, S. S. C., D. Shankar, and S. R. Shetye, 2002: Differences in heat budgets of the near-surface Arabian Sea and Bay of Bengal: Implications for the summer monsoon. *J. Geophys. Res.*, **107**(C6), 5.1–5.14.

Tomitha, T., and T. Yasunari, 1996: Role of the northeast winter monsoon on the biennial oscillation of the ENSO/monsoon system. *J. Meteor. Soc. Japan*, **74**, 399–4213.

Wen, C., H.–T. Graf, and H. Ronghui, 2000: The interannual variability of East Asian winter monsoon and its relation to the summer monsoon. *Adv. Atmos. Sci.*, **17**, 48–60.

Wyrtki, K., 1961: Physical oceanography of southeast ocean waters: Scientific results of marine investigations of the South China Sea and Gulf of Thailand. *NAGA Rep. 2*, Scrippts Institute of Oceanography, La Jolla, California, 195pp.

Xie, S.–P., Q. Xie, D. Wang, and W. T. Liu, 2003: Summer upwelling in the South China Sea and its role in regional climate variations. *J. Geophys. Res.*, **108**(C8)**,** 3261, doi: 10.1029/2003JC001867.